Higher-order topological insulators on porous network models

Ying Han
College of Physics Science and Technology, Yangzhou University, Yangzhou 225002, China
and State Key Laboratory of Surface Physics and Department of Physics, Fudan University, Shanghai 200433, China

Ai-Lei He*
Institute for Advanced Study, Tsinghua University, Beijing 100084, China

(Received 6 April 2021; accepted 12 October 2021; published 20 October 2021)

A prominent characteristic of two-dimensional higher-order topological insulators (2D-HOTIs) is the topologically protected corner modes associated with gapped edge states. Opening the gap of bulk and edge states is a key to realizing 2D-HOTIs. In this paper, we theoretically propose that 2D-HOTIs can be realized on porous network models. We consider two porous network models, the graphenylenelike and the porous-honeycomb models, which respectively contain 12 and 18 atoms in supercells. These superstructures can open the bulk gap as well as the edge gap and induce HOTIs. Experimentally, graphene nanomesh, other 2D porous materials, and organic molecules naturally host supercells with regular nanoholes, which can be candidates to realizing HOTIs. Our studies reveal that 2D-HOTIs can be realized on some 2D porous network models and provide a promising route to explore HOTI states in real materials.

DOI: 10.1103/PhysRevB.104.165416

I. INTRODUCTION

Theoretical predictions and experimental realizations of topological insulators (TIs) have demonstrated the existence of robust boundary states and revealed the bulk-boundary correspondence. Several representative TI models have been theoretically proposed and experimentally achieved, such as quantum anomalous Hall states [1–3], quantum spin Hall (QSH) states [4–6], and topological crystalline insulators [7,8]. Intriguingly, topological states have been explored in some graphene-based systems, such as quasi-one-dimensional graphene nanoribbons with specially designed structures [9–12], Kekulé-distorted graphene [13–15], and porous graphene [16], most of which host supercells. Different from the representative TIs, their topological nature originates from the geometric configurations of superstructures. For example, the topology of quasi-one-dimensional graphene nanoribbon can be destroyed by its edge, width, and end termination [9] and, in the porous graphene, the size and distance of regular holes have an impact on the topological states [16]. For these graphene-based systems, the specially designed supercells with nanoscale can modify the band structures, open a new bulk gap, and finally induce the conventional (or first-order) topological states.

In stark contrast to conventional TIs [17,18], two-dimensional higher-order TIs (2D-HOTIs) host both gapped edge and robust corner states [19–33], which indicates the existence of an anomalous bulk-boundary correspondence, i.e., the bulk-corner correspondence. Consequently, the key to realizing 2D-HOTIs is to open both the bulk and edge gaps and obtain robust corner states. Lattice dimerization in spinless systems [19,20,27,29,30] and in-plane Zeeman field in QSH systems [31–33] can open both bulk and edge gaps and achieve HOTIs—for example, the Benalcazar-Bernevig-Hughes model [19,20] and Kekulé distorted graphene [29,30], in which the HOTIs are characterized by quantized quadrupole momentum. The quadrupole momentum can be calculated on the basis of the nested Wilson loop [19,20] as well as parities at high symmetric points in inversion symmetry protected systems [29]. Numerous 2D-HOTIs models have been proposed theoretically; however, few works report the realization of 2D-HOTIs in real materials. To date, 2D-HOTIs in some real materials have been predicted theoretically, such as the graphdiyne [34,35] and γ graphene [36], on account of the $C-C$ single bonds mixing with the $C \equiv C$ triple bonds, which detunes the nearest-neighbor (NN) hopping potentials, in analogy to Kekulé-distorted bonds.

In this paper, we theoretically propose several 2D porous network models to achieve HOTIs, which are induced by the specially designed supercells instead of lattice dimerization or in-plane magnetic field. We introduce two triangle lattice models with superstructures—the graphenylenelike and porous-honeycomb models, whose supercells contain 12 and 18 atoms, respectively. The present superstructures can open the bulk gap as well as the edge gap, and induce HOTIs. These HOTIs can be characterized by the robust corner states and the quantized bulk quadrupole momentum. Because the present models have inversion symmetry, the bulk quadrupole invariant can be calculated on the basis of parities at high symmetric points [29]. In real materials, graphene nanomesh, other 2D porous materials and some organic molecules naturally possess superstructures, which can be candidates to

*heaileinju@gmail.com

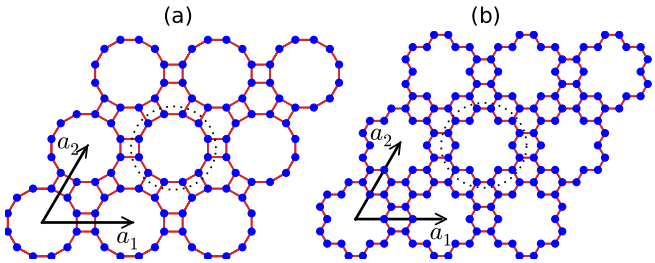

FIG. 1. Schematic structure of graphenylenelike (a) and porous-honeycomb (b) models on a triangle lattice, where the gray dashed circles contain intracellular configuration. In graphenylenelike lattice, there are 12 atoms in a unit cell and 18 atoms as a unit cell in a porous graphene model. The graphenylenelike model differs from the graphenylene [37], for there are two types of NN bonds (C − C single bonds and C = C double bonds) in graphenylene. However, the graphenylenelike model only hosts one type of NN bond with uniform length. Here, a_1 and a_2 are the lattice vectors.

realize 2D-HOTIs. On the other hand, HOTIs can be explored in 2D artificially porous microstructures as well. Our studies shed light on the realization of HOTIs on 2D porous networks and may provide a prospective approach to achieve 2D-HOTIs in real materials.

II. POROUS NETWORK MODELS

Graphene is a semimetal in which the energy bands touch at high symmetric points K and K' [38,39]. However, in porous graphene, the superstructure with regular arrays of nanoholes can induce band gaps and modify the electron propagation [16], for there are no hopping processes in the region of nanoholes. Hopping processes of some specially designed superstructures may open both the bulk and edge gaps. Here, we consider two porous network models on triangle lattice—the graphenylenelike and the porous-honeycomb lattices whose supercells contain 12 and 18 atoms, respectively (shown in Fig. 1). The tight-binding Hamiltonian is given by

$$H = t \sum_{\langle \mathbf{r}\mathbf{r}' \rangle} [a^\dagger_{\mathbf{r}'} a_{\mathbf{r}} + \text{H.c.}], \tag{1}$$

where $a^\dagger_{\mathbf{r}}$ ($a_{\mathbf{r}}$) denotes the creation (annihilation) operator at site $\mathbf{r}$, $\langle \ldots \rangle$ indicates the NN pairs of sites, and t is the NN hopping potential, respectively. For simplicity, we set $t = 1.0$.

The models host both time-reversal symmetry and inversion symmetry, i.e., $\mathcal{T}H(k)\mathcal{T}^\dagger = H(-k)$ and $\mathcal{P}H(k)\mathcal{P}^\dagger = H(-k)$, where $H(k)$ is the Hamiltonian in momentum space and $\mathcal{T}$ and $\mathcal{P}$ denote the time-reversal and inversion operators, respectively. On account of the time-reversal symmetry, Berry curvature satisfies $\mathcal{F}(-\mathbf{k}) = -\mathcal{F}(\mathbf{k})$, but the inversion symmetry requires $\mathcal{F}(-\mathbf{k}) = \mathcal{F}(\mathbf{k})$. Consequently, the Berry curvature is $\mathcal{F} = 0$ everywhere in the Brillouin zone, which is in sharp contrast to Chern insulators and QSH states [40]. Chern numbers of these two porous models naturally equal zero for $\mathcal{C} = \frac{1}{2\pi} \int_{BZ} d^2\mathbf{k}\, \mathcal{F}(\mathbf{k})$ [41].

III. ENERGY BANDS AND GAPPED EDGE STATES

By Fourier transformation and numerical diagonalization of the Hamiltonian of both lattice models on torus geometry,

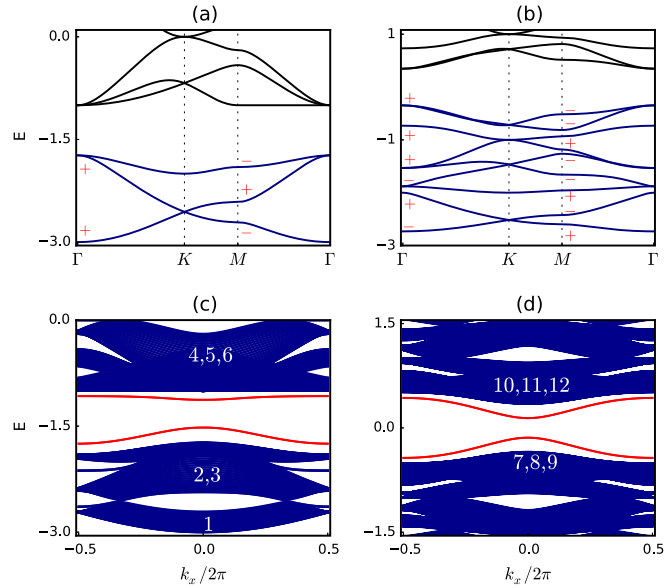

FIG. 2. Energy bands of the present models. Bulk energy bands on torus geometry are shown in (a) graphenylenelike model and (b) porous-honeycomb model. The parities at high symmetric points are marked in the bands with "+" or "−." Energy bands on cylinder geometry of both lattice models are shown in (c) and (d). Gapped edge states emerge and are marked with red. We also mark the bands with numbers "1," "2," "3,"....

we obtain the bulk energy spectrum in the first Brillouin zone (shown in Fig. 2). For the graphenylenelike model [shown in Fig. 1(a)], the bulk gap opens between the third and the fourth bands [at quarter filling, shown in Fig. 2(a)]. In the porous-honeycomb model [shown in Fig. 1(b)], the bulk energy bands are gapped at half filling. On account of both models with inversion symmetry, we can obtain the parities (the eigenvalue of inversion operator $\mathcal{P}$) $\eta = +1$ or -1. Based on these parities, the dipole invariant $\mathbf{p} = (p_x, p_y)$ can be expressed as [40]

$$p_i = \sum p_i^n, \quad p_i^n = \frac{1}{2}\left(q_i^n \bmod 2\right), \quad (-1)^{q_i^n} = \frac{\eta^n(M)}{\eta^n(\Gamma)}, \tag{2}$$

where η^n indicates the parity of the nth band and $i = x$ or y is the direction of the reciprocal lattice vector. The quadrupole momentum Q is defined based on the dipole momentum of the nth band p_i^n [29],

$$Q_{ij} = \sum_n p_i^n p_j^n. \tag{3}$$

The quantized quadrupole momentum associated with zero dipole momentum [29] can be used to identify the HOTIs in several triangle lattice models with inversion symmetry, such as the Kekulé-distorted graphene [29], the γ graphene [36], etc.

The energy bands of both models on cylinder geometry are illustrated in Figs. 2(c) and 2(d). There are clear edge states in the energy gap. Simultaneously, the edge states are gapped, which is reminiscent of the 2D-HOTIs. In order to identify these novel edge-gapped states, we calculate the quadrupole invariant Q_{xy} defined in Eq. (3). We first obtain the diploe momentum (p_x, p_y) of both lattice models with the aid of par-

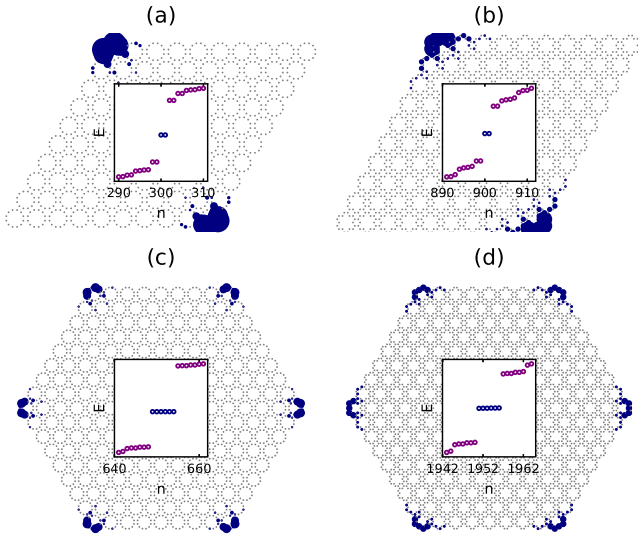

FIG. 3. Density profiles of topological states localized around corners. Here, we consider the graphenylenelike (a),(c) and porous-honeycomb (b),(d) lattice models on parallelograms and hexagonal-shaped planes. The inset of every figure displays part of the energy eigenvalues, including obtuse corner states (colored with blue), acute corner states, and edge states (colored with purple).

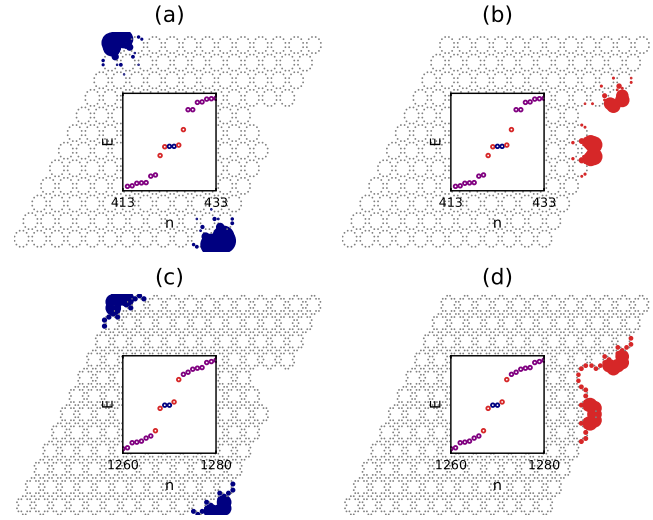

FIG. 4. Robust corner states against defects. Panels (a) and (c) display the corner states localized around obtuse parts. Panels (b) and (d) show the corner states around corners induced by the defects. The inset in every figure displays part of the energy eigenvalues, including obtuse corner states (colored with blue), corner states around defects (colored with red), and edge states (colored with purple).

ities at high symmetric points [shown in Figs. 2(a) and 2(b)]. Even though the bulk energies are degenerate at Γ point in our present models, the eigenvalues of inversion symmetry at degenerate bands are the same [shown in Figs. 2(a) and 2(b)]. These degenerate energy bands with the same parity have been reported in Refs. [29,36]. We find the total dipole momentum of both models are vanished, i.e., $(p_x, p_y) = (0, 0)$. According to Eq. (3), we obtain the total quadrupole momentum of the present models as $Q_{xy} = 1/2$, which indicates the existence of HOTI states on these porous network models.

IV. ROBUST CORNER STATES

In stark contrast to the conventional TIs, 2D-HOTIs satisfy bulk-corner correspondence. The present edge-gapped states are identified as a HOTI state on the basis of the quantized bulk quadrupole momentum. Consequently, topologically protected states emerge at corners with open boundary condition. By numerically diagonalizing the Hamiltonian [Eq. (1)] of both models with open boundary condition in real space, we can obtain the energy spectra and density distributions. The density profiles of the topologically protected corner states are illustrated in Fig. 3 on the parallelograms and hexagonal-shaped planes. Here, these corner states are identified with the help of the energy spectra (the inset ones in Fig. 3). Both the lattice models in parallelograms host twofold degenerate corner states [displayed in the insets of Figs. 3(a) and 3(b)], which are localized around the corners with obtuse angles, in analogy to the graphdiyne [34,35] and γ graphene [36]. From the insets of Figs. 3(c) and 3(d), we find there are sixfold degenerate states localized around the corners of these models in hexagonal-shaped planes. In addition, the corner states can also emerge around the acute corners. We present the acute corner states and the edge states (colored with purple in Fig. 3) in Appendix A.

In 2D-HOTIs, topologically protected corner states are very robust to defects or disorders, unless the strong defects or disorders completely destroy the corners. We consider the lattice model with a defect (shown in Fig. 4). By exact diagonalization of the real-space Hamiltonian, we obtain the corner states around obtuse parts [shown in Figs. 4(a) and 4(c)], which suggest that corner states are robust against the defects. Moreover, we find several localized corner states are around the defects [shown in Figs. 4(b) and 4(d)] on account of the appearance of corners, which stresses once more the existence of topologically protected corner states in both present models.

These robust corner states originate from the domain wall states at the intersection of two edges because of the different hopping processes along the edge or the corner. For simplicity, we display the various hopping processes of the graphenylenelike model in schematic Fig. 5. Along the edge (with the same direction), there are five hopping processes in every unit cell (details in Fig. 5) and seven hopping processes along the corner. These different hopping processes can create a robust domain wall state and the similar origin of topological corner states has been reported in graphdiyne and γ graphyne. For the porous-honeycomb model, there is also a domain wall emerging at corners. Simultaneously, we find these corner states do not exactly require the crystalline symmetries, such as threefold rotational symmetry (C_3), sixfold rotational symmetry (C_6), inversion symmetry ($\mathcal{P}$), and mirror symmetry ($\mathcal{M}$) (details in Appendix C), which means that the corner states remain present when breaking C_3, C_6, $\mathcal{P}$, and $\mathcal{M}$ symmetry. The corner states, as domain-wall modes between two edges, must be robust against the perturbations. These robust corner states have emerged in the graphdiyne and

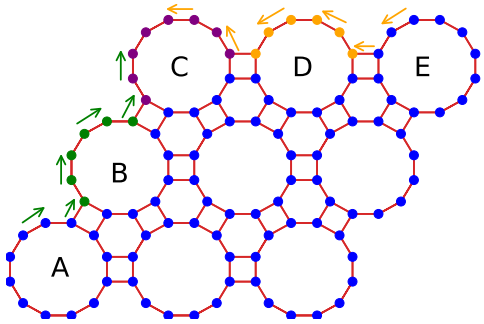

FIG. 5. Schematic figure of the domain wall states at the intersection of two edges in a graphenylenelike model. There are five hopping processes along the edge colored with green and orange; however, there are seven hopping processes at the corner. A domain wall emerges which can localize the corner state. Meanwhile, the arrows denote the hopping processes along one direction and an electron can hop against the arrows as well.

the γ graphyne models protected without crystalline symmetries. Even though the present HOTI is not required inversion symmetry, the quadrupole momentum can still be calculated based on the parities in the systems with inversion symmetry.

These corner states do not depend on the crystalline symmetries; however, opening bulk and edge gap is very necessary. For these porous models, HOTI stems from the specially designed supercells, instead of the lattice dimerization, which is in contrast to Kekulé graphene and breathing Kagome lattice. However, tuning the lattice dimerization may lead to other phases. Hence we also explore the topological phase transition by tuning the intercellular hopping process t_1 (details in Fig. 6). For these two porous network models, when t_1 is smaller than 0.5, the phase belongs to the normal insulator; however, when t_1 is larger than 0.5, the HOTI phase emerges. By tuning t_1, there are only two phases appearing, and this HOTI phase can be characterized by the robust corner state and the quantized quadrupole momentum.

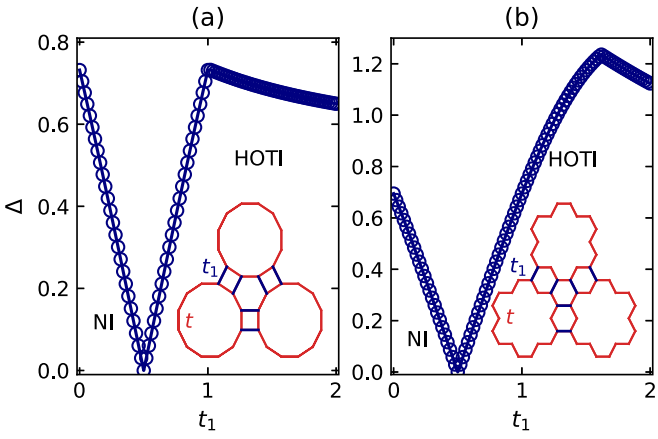

FIG. 6. Topological phase transitions of these two porous network models. Δ is the band gap. "*NI*" and "*HOTI*" denote the normal insulator phase and the higher-order topological phase, respectively. The insets display the structure of graphenylenelike and porous-honeycomb models with intracellular hopping process t and intercellular hopping process t_1.

V. HOTIs IN GRAPHENE NANOMESH

We have demonstrated the existence of HOTIs in two porous network models, the graphenylenelike and the porous-honeycomb lattices. In real materials, graphene nanomesh as a type of carbon network may be a candidate to realizing HOTIs. Graphene nanomesh belongs to the porous lattice with regular nanoholes in a graphene sheet [42–44], which hosts superstructures. Experimentally, nanoholes in graphene nanomesh [44] can be specially designed by manually tuning the size of nanoholes, the distance between two nanoholes, etc. Here, we model three graphene nanomesh structures with various sizes of nanoholes [shown in Figs. 7(a)–7(c)] using a tight-binding description. We set $t = -2.8$ eV, which is the NN hopping integral in graphene. The energy bands on torus geometry are obtained by numerically diagonalizing the Hamiltonian [in Eq. (1)]. We find the bulk gaps of these models are opened at half filling, which indicates the appearance of insulator states. Simultaneously, parities of each band can be respectively calculated with the marked signs "+" or "−" displayed in Figs. 7(d)–7(f). According to the definition of dipole and quadrupole momentum [in Eqs. (2) and (3)], we can obtain the vanished dipole momentum and quantized quadrupole momentum $Q_{xy} = 1/2$ of these three models at half filling, suggesting the existence of HOTIs. Furthermore, the robust corner states are displayed in Appendix C.

Different from the graphdiyne [34,35] and γ graphene [36], there is no lattice dimerization or bond distorted in graphene nanomeshes. In specially designed graphene nanomeshes, superstructures can open both the bulk and edge gaps and induce HOTIs. Consequently, we provide a promising scheme to realize 2D-HOTIs. Based on our proposals, experimentally, graphene nanomeshes can be a potential candidate to realizing 2D-HOTI. Besides graphene, numerous 2D materials have been discovered, such as silicene [45], germanene [46], arsenene [47], antimonene [48], borophene [49], etc. Consequently, 2D-HOTIs can be realized in other 2D porous materials as well. On the other hand, several organic materials naturally host superstructures, such as polycyclic aromatic hydrocarbons [50], annulenes [51], and fullerenes [52], which can be used to realize HOTIs. Besides real materials, porous network models can be simulated in some 2D artificial microstructures and the HOTIs may be realized in these artificial porous networks.

VI. SUMMARY AND DISCUSSION

We theoretically propose a feasible scheme to realize HOTIs on 2D porous networks. We consider two porous network models on a triangle lattice—the graphenylenelike and the porous-honeycomb models. These supercells with specially designed nanoholes can open the bulk gap as well as the edge gap, which induce HOTIs. These HOTIs can be characterized by robust corner states and quantized quadrupole invariant. In real materials, we investigate the band structure of graphene nanomesh and demonstrate the appearance of HOTIs which are induced by superstructures. The geometric configuration of supercells plays a crucial role in our models, and the present

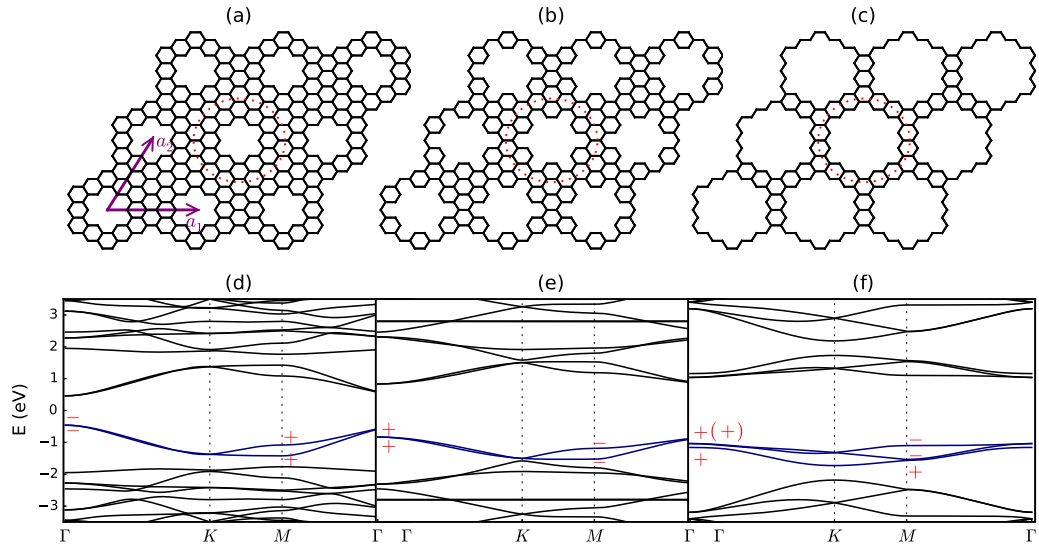

FIG. 7. Graphene nanomesh models and their bulk energy bands. (a)–(c) Crystal structures of graphene with regular nanoholes in a triangle lattice. The red circles contain several intracellular configurations which are viewed as supercells. Gray lines with arrows denote the lattice vectors and are marked with a_1 and a_2. Panels (d)–(f) show the bulk energy bands on torus geometry marked with signs of parities at high symmetric points. The parities at high symmetric points are marked with "+" or "−."

idea can be extended to other 2D materials which naturally host superstructures as well.

Our findings can open up several future research paths on 2D materials with superstructures. First, flat bands have been reported in porous graphene [53]. Exploration of topological flat bands and strongly correlated physics in porous models will be a significant issue. There are three narrow bands in Fig. 7(f), colored with blue. By tuning the hopping parameters or the geometry of nanoholes, a nearly topological flat band is possibly acquired. Secondly, charge fractionalization has been investigated in HOTIs [19,20]. Theoretical and experimental explorations on fractional charge in porous systems may be another attractive issue. Thirdly, an interesting property of 2D HOTIs is the existence of the one-dimensional symmetry protected topological phase on the boundary, for example, the Benalcazar-Bernevig-Hughes model [19,20]. One-dimensional symmetry protected topological phases may

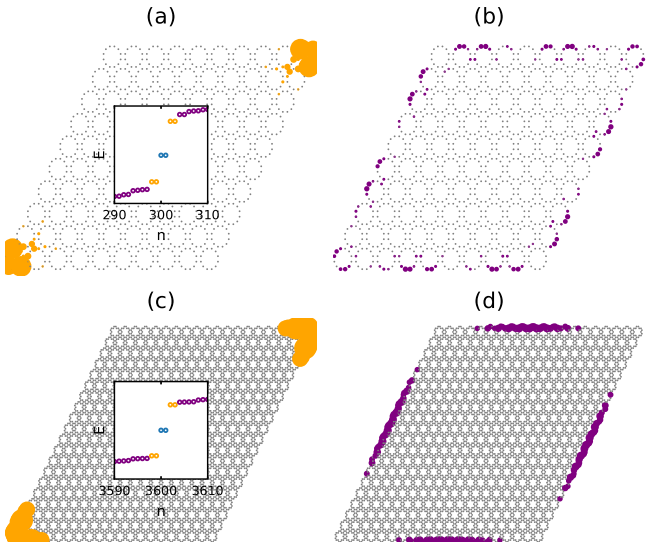

FIG. 8. Boundary states in graphenylenelike and porous-honeycomb models. (a) Acute corner states and (b) edge states in the graphenylenelike model. (c) Acute corner states and (d) edge states in the porous-honeycomb model. The inset in every figure displays energy eigenvalues of obtuse corner states (colored with blue), acute corner states (colored with orange), and edge states (colored with purple).

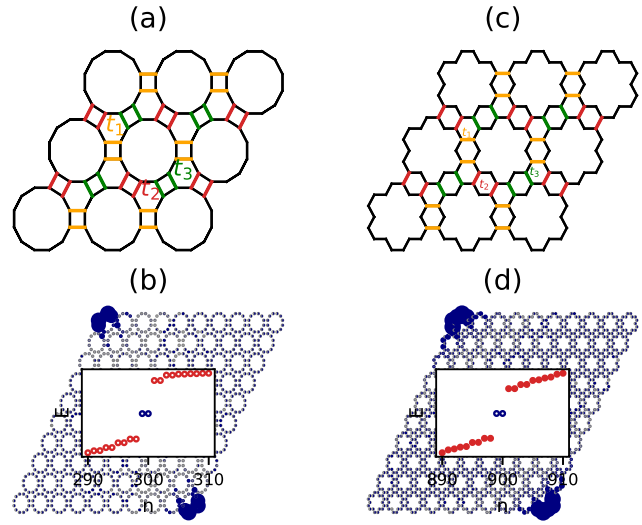

FIG. 9. Robust corner states against C_3 and C_6 symmetries. (a) Anisotropically intercellular hopping processes (t_1, t_2, and t_3) in the graphenylenelike model and the robust corner state is displayed in (b). (c) Anisotropically intercellular hopping processes (t_1, t_2, and t_3) in the porous-honeycomb model and the robust corner state is displayed in (d). The insets in (b) and (d) denote energy eigenvalues of corner states. Here, along the black bonds, the hopping potential is $t = 1$. We choose $t_1 = 1.2$, $t_2 = 1.0$, and $t_3 = 0.8$ for these two models.

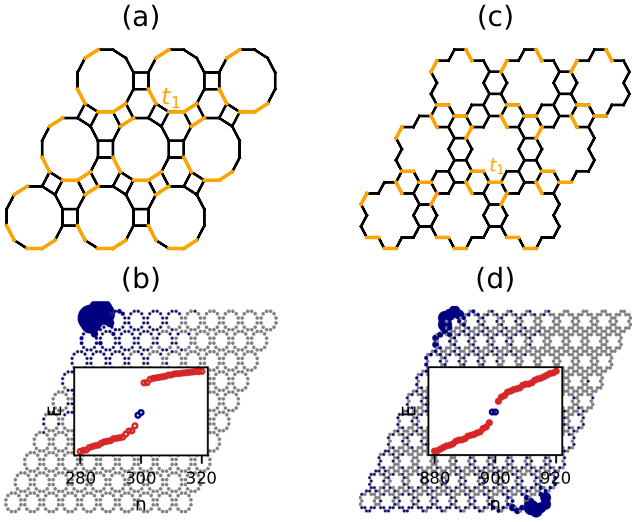

FIG. 10. Robust corner states against inversion and mirror symmetries. (a) Anisotropically intracellular hopping processes (t_1) in the graphenylenelike model and the robust corner state is displayed in (b). (c) Anisotropically intracellular hopping processes (t_1) in the porous-honeycomb model and the robust corner state is displayed in (d). The insets in (b) and (d) denote energy eigenvalues of corner states. Here, along the black bonds, the hopping potential is $t = 1$. We choose $t_1 = 0.9$ for these two models.

appear in some 2D porous network models. Lastly, the geometry and irregular arrangement of nanoholes may have an impact on topological states. Which types of superstructures can host topological states remains unclear.

ACKNOWLEDGMENTS

This work is supported in the project funded by China Postdoctoral Science Foundation (Grant No. 2020M680499).

APPENDIX A: BOUNDARY STATES IN GRAPHENYLENELIKE AND POROUS-HONEYCOMB MODELS

We have shown the real-space density distribution of the robust corner states in graphenylenelike and porous-honeycomb models and these corner states with twofold degeneracy in both models. Here, we show the corner states localized around the acute parts of lattices in real space in Figs. 8(a) and 8(c). These acute corner states host twofold degeneracy as well. Except for the corner states, edge states appear in the energy spectra [as shown in Figs. 8(a) and 8(c)]. We also display the density distributions of the edge states for these two models in Figs. 8(b) and 8(d).

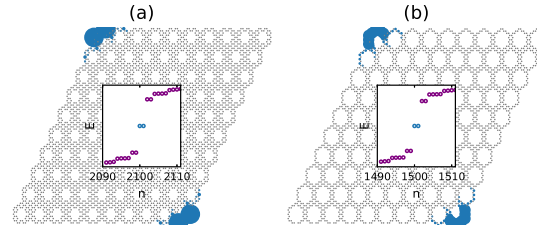

FIG. 11. Robust corner states in graphene nanomesh. There are 42 and 30 atoms in CICGs of (a) and (b), respectively. The inset in every figure displays energy eigenvalues of corner states (colored with blue).

APPENDIX B: ROBUST CORNER STATES WITHOUT CRYSTALLINE SYMMETRIES

In the main text, we argue that the present HOTIs originate from the topological domain wall states and do not depend on the crystalline symmetries. Here, we show these robust corner states emerge in systems without C_3, C_6, $\mathcal{P}$, and $\mathcal{M}$ symmetries. First, we consider models with anisotropically intercellular hopping potentials along various directions [different hopping potentials t_1, t_2, and t_3 shown in Figs. 9(a) and 9(c)]. Both the models are absent of C_3 and C_6 symmetries; however, the robust corner states are still localized around corners [displayed in Figs. 9(b) and 9(d)], which manifest these HOTI states and are not protected by C_3 and C_6 symmetries. Secondly, we tune the anisotropically intracellular hopping potentials [details shown in Figs. 10(a) and 10(c)] which break the inversion and mirror symmetry in both models. Nevertheless, the corner states still exist, which suggests these HOTIs do not depend on the inversion and mirror symmetry.

APPENDIX C: ROBUST CORNER STATES IN GRAPHENE NANOMESH

HOTIs have been theoretically predicted in porous graphenes on the basis of the gapped edge states on cylinder geometry and quantized quadrupole invariant on torus geometry. Here, we choose graphene nanomesh with 42 and 30 atoms and consider the density distribution of corner states. We numerically diagonalize the real-space Hamiltonian with open boundary and obtain the energy spectra and sing-particle states. Twofold degeneracy zero-energy states emerge in the gap which suggests the existence of corner states of both models. We display the density distribution of these zero-energy states in Fig. 11 and they are indeed the corner states; most of the densities are localized around corners. These numerical results reveal the existence of HOTIs again in graphene nanomesh.

[1] F. D. M. Haldane, Phys. Rev. Lett. **61**, 2015 (1988).
[2] C.-Z. Chang, J. Zhang, X. Feng, J. Shen, Z. Zhang, M. Guo, K. Li, Y. Ou, P. Wei, L.-L. Wang, Z.-Q. Ji, Y. Feng, S. Ji, X. Chen, J. Jia, X. Dai, Z. Fang, S.-C. Zhang, K. He, Y. Wang *et al.*, Science **340**, 167 (2013).
[3] G. Jotzu, M. Messer, R. Desbuquois, M. Lebrat, T. Uehlinger, D. Greif, and T. Esslinger, Nature (London) **515**, 237 (2014).
[4] C. L. Kane and E. J. Mele, Phys. Rev. Lett. **95**, 226801 (2005).
[5] B. A. Bernevig, T. L. Hughes, and S.-C. Zhang, Science **314**, 1757 (2006).

[6] M. König, S. Wiedmann, C. Brüne, A. Roth, H. Buhmann, L. W. Molenkamp, X.-L. Qi, and S.-C. Zhang, Science **318**, 766 (2007).
[7] L. Fu, Phys. Rev. Lett. **106**, 106802 (2011).
[8] Y. Tanaka, Z. Ren, T. Sato, K. Nakayama, S. Souma, T. Takahashi, K. Segawa, and Y. Ando, Nat. Phys. **8**, 800 (2012).
[9] T. Cao, F. Zhao, and S. G. Louie, Phys. Rev. Lett. **119**, 076401 (2017).
[10] G. Tamaki, T. Kawakami, and M. Koshino, Phys. Rev. B **101**, 205311 (2020).
[11] D. J. Rizzo, G. Veber, T. Cao, C. Bronner, T. Chen, F. Zhao, H. Rodriguez, S. G. Louie, M. F. Crommie, and F. R. Fischer, Nature (London) **560**, 204 (2018).
[12] O. Gröning, S. Wang, X. Yao, C. A. Pignedoli, G. Borin Barin, C. Daniels, A. Cupo, V. Meunier, X. Feng, A. Narita, K. Müllen, P. Ruffieux, and R. Fasel, Nature (London) **560**, 209 (2018).
[13] L.-H. Wu and X. Hu, Phys. Rev. Lett. **114**, 223901 (2015).
[14] L.-H. Wu and X. Hu, Sci. Rep. **6**, 24347 (2016).
[15] T. Kariyado and X. Hu, Sci. Rep. **7**, 16515 (2017).
[16] T. Kariyado, Y.-C. Jiang, H. Yang, and X. Hu, Phys. Rev. B **98**, 195416 (2018).
[17] M. Z. Hasan and C. L. Kane, Rev. Mod. Phys. **82**, 3045 (2010).
[18] X.-L. Qi and S.-C. Zhang, Rev. Mod. Phys. **83**, 1057 (2011).
[19] W. A. Benalcazar, B. A. Bernevig, and T. L. Hughes, Science **357**, 61 (2017).
[20] W. A. Benalcazar, B. A. Bernevig, and T. L. Hughes, Phys. Rev. B **96**, 245115 (2017).
[21] Z. Song, Z. Fang, and C. Fang, Phys. Rev. Lett. **119**, 246402 (2017).
[22] J. Langbehn, Y. Peng, L. Trifunovic, F. von Oppen, and P. W. Brouwer, Phys. Rev. Lett. **119**, 246401 (2017).
[23] F. Schindler, A. M. Cook, M. G. Vergniory, Z. Wang, S. S. P. Parkin, B. A. Bernevig, and T. Neupert, Sci. Adv. **4**, 0346 (2018).
[24] M. Ezawa, Phys. Rev. B **98**, 045125 (2018).
[25] W. A. Benalcazar, T. Li, and T. L. Hughes, Phys. Rev. B **99**, 245151 (2019).
[26] S. Franca, J. van den Brink, and I. C. Fulga, Phys. Rev. B **98**, 201114(R) (2018).
[27] M. Ezawa, Phys. Rev. Lett. **120**, 026801 (2018).
[28] L. Trifunovic and P. W. Brouwer, Phys. Rev. X **9**, 011012 (2019).
[29] F. Liu, H.-Y. Deng, and K. Wakabayashi, Phys. Rev. Lett. **122**, 086804 (2019).
[30] E. Lee, A. Furusaki, and B.-J. Yang, Phys. Rev. B **101**, 241109(R) (2020).
[31] M. Ezawa, Phys. Rev. Lett. **121**, 116801 (2018).
[32] Y. Ren, Z. Qiao, and Q. Niu, Phys. Rev. Lett. **124**, 166804 (2020).
[33] C. Chen, Z. Song, J.-Z. Zhao, Z. Chen, Z.-M. Yu, X.-L. Sheng, and S. A. Yang, Phys. Rev. Lett. **125**, 056402 (2020).
[34] E. Lee, R. Kim, J. Ahn, and B.-J. Yang, npj Quantum Mater. **5**, 1 (2020).
[35] X.-L. Sheng, C. Chen, H. Liu, Z. Chen, Z.-M. Yu, Y. X. Zhao, and S. A. Yang, Phys. Rev. Lett. **123**, 256402 (2019).
[36] B. Liu, G. Zhao, Z. Liu, and Z. F. Wang, Nano Lett. **19**, 6492 (2019).
[37] A. T. Balaban and K. P. C. Vollhardt, Open Org. Chem. J. **5**, 117 (2011).
[38] A. H. Castro Neto, F. Guinea, N. M. R. Peres, K. S. Novoselov, and A. K. Geim, Rev. Mod. Phys. **81**, 109 (2009).
[39] S. Das Sarma, S. Adam, E. H. Hwang, and E. Rossi, Rev. Mod. Phys. **83**, 407 (2011).
[40] F. Liu and K. Wakabayashi, Phys. Rev. Lett. **118**, 076803 (2017).
[41] D. J. Thouless, M. Kohmoto, M. P. Nightingale, and M. den Nijs, Phys. Rev. Lett. **49**, 405 (1982).
[42] N. Shima and H. Aoki, Phys. Rev. Lett. **71**, 4389 (1993).
[43] T. G. Pedersen, C. Flindt, J. Pedersen, N. A. Mortensen, A.-P. Jauho, and K. Pedersen, Phys. Rev. Lett. **100**, 136804 (2008).
[44] J. Bai, X. Zhong, S. Jiang, Y. Huang, and X. Duan, Nat. Nanotechnol. **5**, 190 (2010).
[45] B. Aufray, A. Kara, S. Vizzini, H. Oughaddou, C. Léandri, B. Ealet, and G. Le Lay, Appl. Phys. Lett. **96**, 183102 (2010).
[46] M. E. Dávila, L. Xian, S. Cahangirov, A. Rubio, and G. L. Lay, New J. Phys. **16**, 095002 (2014).
[47] C. Kamal and M. Ezawa, Phys. Rev. B **91**, 085423 (2015).
[48] S. Zhang, Z. Yan, Y. Li, Z. Chen, and H. Zeng, Angew. Chem. Int. Ed. Engl. **54**, 3112 (2015).
[49] A. J. Mannix, X.-F. Zhou, B. Kiraly, J. D. Wood, D. Alducin, B. D. Myers, X. Liu, B. L. Fisher, U. Santiago, J. R. Guest, M. J. Yacaman, A. Ponce, A. R. Oganov, M. C. Hersam, and N. P. Guisinger, Science **350**, 1513 (2015).
[50] G. Rhodes, R. B. Opsal, J. T. Meek, and J. P. Reilly, Anal. Chem. **55**, 280 (1983).
[51] S. M. Johnson, I. C. Paul, and G. S. D. King, J. Chem. Soc. B 643 (1970).
[52] H. W. Kroto, J. R. Heath, S. C. O'Brien, R. F. Curl, and R. E. Smalley, Nature (London) **318**, 162 (1985).
[53] M. Vanević, V. M. Stojanović, and M. Kindermann, Phys. Rev. B **80**, 045410 (2009).